Applied Surface Science 403 (2017) 500–508

Contents lists available at ScienceDirect

Applied Surface Science

journal homepage: www.elsevier.com/locate/apsusc

Full Length Article

Effects of metals doping on the removal of Hg and H_2S over ceria

Lixia Ling[a], Zhongbei Zhao[a], Senpeng Zhao[a], Qiang Wang[c], Baojun Wang[b,*], Riguang Zhang[b], Debao Li[c]

[a] College of Chemistry and Chemical Engineering, Taiyuan University of Technology, Taiyuan 030024, Shanxi, People's Republic of China
[b] Key Laboratory of Coal Science and Technology (Taiyuan University of Technology), Ministry of Education and Shanxi Province, Taiyuan 030024, Shanxi, People's Republic of China
[c] State Key Laboratory of Coal Conversion, Institute of Coal Chemistry, Chinese Academy of Sciences, Taiyuan 030001, Shanxi, People's Republic of China

ARTICLE INFO

Article history:
Received 16 November 2016
Received in revised form
19 December 2016
Accepted 13 January 2017
Available online 15 January 2017

Keywords:
Metal doping
Hg removal
H_2S removal
Ceria
Density functional theory

ABSTRACT

The effects of Mn and Fe doping into the $CeO_2(111)$ surface on the simultaneous removal of Hg and H_2S was investigated, a density functional theory calculation with the on-site Coulomb interaction taken into account was adopted. The adsorptions of Hg-containing species on perfect $CeO_2(111)$, $Mn/CeO_2(111)$ and $Fe/CeO_2(111)$ surfaces were studied, the results showed that Mn and Fe dopants facilitated Hg adsorption, and more charge transferred from Hg atom to the metal doped surfaces; HgS preferred to adsorb on the perfect surface with the dissociated mode, while with the molecular mode on $Mn/CeO_2(111)$ and $Fe/CeO_2(111)$ surfaces. The reaction mechanism show that the dissociated S by H_2S can easily react with Hg leading to the formation of HgS on $Mn/CeO_2(111)$ and $Fe/CeO_2(111)$ surfaces, which is crucial to capture mercury.

1. Introduction

Mercury is a major heavy metal pollutant in coal-derived gas [1–3], and H_2S is a main sulfur-containing pollutant [4]. They have adverse effects on environment and human health [5]. Importantly, elemental Hg is difficult to remove due to the chemical inertness and structural stability [6,7], and H_2S shows significant negative impacts on catalyst performance [8]. Thus they must be removed from coal-derived gas. Ceria has been attracting more attention due to its excellent physical and chemical properties, and has been used in catalytic field [9–11]. In addition, CeO_2 not only has good desulfurization properties [12–14], but also can effectively remove mercury [15–18]. However, the simultaneous removal ability of Hg and H_2S for CeO_2 is not clear.

The introduction of a second metal into CeO_2 can effect its structure and properties, such as redox properties [19] and chemical catalytic performances [20]. Previous work also showed that CeTi sorbent with a CeO_2/TiO_2 mass ratio of 0.2 exhibited superior elemental Hg removal efficiency, and H_2S was the most effective syngas component and helpful for Hg removal. HgS was formed by active surface sulfur generated from H_2S reacting with gas-phase Hg via Eley-Rideal mechanism [21]. Transition metals were commonly used as modified elements to improve the catalytic performance of metal oxide [22–25]. The effect of Mn/Fe-dopant on facilitating surface oxygen vacancies formation on CeO_2 surface was investigated [26,27], which promoted CO oxidation leading to the formation of CO_2 [26,28]. Mn-doping on the $CeO_2(111)$ surface also promoted C—H bond activation during the propane oxidation because Mn atoms served as reduction centers. Mn-doping led to oxygen vacancy formation and Mn^{4+} reduction to Mn^{3+}, and then propane activation led to Mn further reducing from Mn^{3+} to Mn^{2+} [29]. A similar result was obtained by CH_4-temperature programmed surface reaction (CH_4-TPSR) and CO-TPSR for the oxidation of CH_4 and CO over $Ce_{0.9}Fe_{0.1}O_2$ catalyst, in which the oxygen vacancies were easily formed and lattice oxygen easily migrated, would contribute to the oxidation [30]. The Lewis acid sites have an important role in the reaction of NH_3. The adsorption and oxidation of NH_3 on Fe, Mn, La and Y doped CeO_2 were studied by DFT calculations, the higher NH_3 activation was investigated on the Fe/CeO_2 and Mn/CeO_2 catalysts than that on La/CeO_2 and Y/CeO_2. More NH_3 adsorption sites on the Lewis acid for Fe/CeO_2 and Mn/CeO_2 catalysts were responsible for the high NH_3 oxidation activation [20]. For the selective catalytic reduction of NO with NH_3, the doping of Fe into CeO_2 led to a decrease of activation energy from 52.0 to

* Corresponding author at: No. 79 West Yingze Street, Taiyuan 030024, People's Republic of China.
E-mail addresses: linglixia@tyut.edu.cn (L. Ling), wangbaojun@tyut.edu.cn (B. Wang).

http://dx.doi.org/10.1016/j.apsusc.2017.01.126
0169-4332/

26.0 kJ mol^{-1}. Because the specific Fe—O—Ce structure was formed and demonstrated by XPS and DFT calculations, which provided more Lewis acid sites and enhanced the redox properties through the electronic inductive effect between Fe^{3+} and Ce^{4+} [9]. It can be seen that doped the second metal can change the properties of metal oxides. And the effect of Mn and Fe doped into CeO_2 surface on the removal of Hg and H_2S is needed to be discussed.

In this work, the adsorptions of Hg-containing species on perfect and Mn/Fe doped CeO_2(111) surfaces are first studied, and the effect of doped metal on the adsorptions will be discussed. And then, the oxidation reaction of Hg by active S will be explored to discuss the simultaneous removal of Hg and H_2S on ceria-based catalysts.

2. Computational details

2.1. Computational methods

A density functional theory (DFT) calculation in a plane-wave basis with the Vienna ab initio simulation package (VASP) code [31,32] was performed. The generalized gradient approximation (GGA) with the Perdew-Burke-Ernzerhof (PBE) [33] exchange-correlation functional was used in this work. The core-valence interaction was described by the projector-augmented wave (PAW) method [34,35] and a cutoff energy of 400 eV was used. To improve the description of the on-site Coulomb interactions in the Ce 4f, Mn 3d and Fe 3d states, spin-polarized DFT + U calculations with U Hubbard values of 5.0 eV for Ce [36,37], 4.5 eV for Mn [38,39] and 4.3 eV for Fe [40,41] were applied. The calculations were carried out using the Brillouim zone sampled with $6 \times 6 \times 6$ and $3 \times 3 \times 1$ Monkhorst-Pack mesh k-points grid for bulk and surface calculations, respectively. The force on all the relaxed atoms was set to 0.02 eV Å^{-1}. Meanwhile, we used the Gaussian smearing method with SIGMA = 0.2 eV to improve convergence of states near the Fermi level. The optimized lattice parameter of ceria bulk is 5.438 Å, which is in good agreement with the experimental value of 5.411 Å [42] and other calculated values [43,44]. The equilibrium geometries of the isolated HgS and H_2S were optimized in a cubic cell of $10 \times 10 \times 10$ Å^3, and the bond lengths of S—H in H_2S are 1.349 and 1.350 Å, which are in line with the experimental data of 1.336 Å [45].

Transition states (TSs) for the elementary reaction were located using the Climbing-image Nudged Elastic Band method (CI-NEB) [46,47], and which were optimized using the dimer method [48,49]. The activation energy (E_a) was defined as the total energy difference between the transition state and the corresponding initial stable structure, is as following equation:

$$E_a = E_{TS} - E_R$$

The adsorption energy (E_{ads}) was defined as:

$$E_{ads} = E_{adsorbate+surface} - E_{surface} - E_{absorbate}$$

Where $E_{adsorbate+surface}$ is the total energy of the system involving the perfect CeO_2(111) or Mn/Fe-doped CeO_2(111) with the adsorbed molecule, $E_{surface}$ and $E_{adsorbate}$ are total energies of different surfaces and the molecule in the gas phase.

2.2. Surface model

The perfect CeO_2(111) surface was constructed by the optimized bulk CeO_2, consisting of a $p(3 \times 3)$ supercell and nine atomic layers (three trilayers), as shown in Fig. 1a and b. Six different adsorption sites can be seen in Fig. 1b. Mn/Fe-doped CeO_2 (111) surfaces (Fig. 1c and d) are built by substituting one Mn or Fe atom for one Ce atom on the first surface. O1 atoms on the first layer used to bond with Ce on the perfect CeO_2(111) surface, while now bond with the doped Mn or Fe on Mn/Fe-doped CeO_2(111) surfaces. The previous theoretical and experimental results have demonstrated that Mn and Fe can enter the lattice structure of CeO_2 and replace the Ce cation [19,38]. A vacuum space of 15 Å was employed to separate each slab from interactions. The bottom three layers were fixed at the optimized bulk positions and the other atoms were allowed to relax.

Table 1
The adsorption energies of Hg and HgS on the perfect CeO_2(111) surface.

	E_{ads}(kJ mol^{-1})		E_{ads}(kJ mol^{-1})
Hg(a)	−4.6	HgS(a)	−53.6
Hg(b)	−2.0	HgS(b)	−41.1
Hg(c)	−3.4	HgS(c)	−118.5
Hg(d)	−3.1	HgS(d)	−91.0
		HgS(e)	−113.6
		HgS(f)	−185.1
		HgS(g)	−194.3
		HgS(h)	−194.2

3. Results and discussion

3.1. Adsorption of Hg species on the perfect CeO_2(111) surface

3.1.1. Hg adsorption on the perfect CeO_2(111) surface

Six different adsorption sites on the perfect CeO_2(111) surface as shown in Fig. 1b are considered for the adsorption of Hg, and optimized structures are shown in Fig. 2. It can be concluded that the interaction between Hg and the surface is quite weak from Table 1, belonging to physical adsorption with an adsorption energy of −4.6 kJ mol^{-1}. It is consistent with the experimental [50] and theoretical results [51]. The most stable adsorption structure is that atomic Hg adsorbs at the top of surface Ce with the Hg-Ce bond of 3.761 Å. The Hg-metal interaction is similar to the adsorption of Hg on the ZnO(10$\bar{1}$0) [52], α-Fe_2O_3(001) [53], CuO(110) [54] and CuO(111) [55] surfaces.

3.1.2. HgS adsorption on the perfect CeO_2(111) surface

Hg is physically adsorbed on the perfect CeO_2(111) surface, implying that Hg can not be removed efficiently. The active S dissociated by H_2S in flue gas may promote the removal of Hg via oxidizing it to HgS [5,52,56–58]. Thereby the adsorption mechanism of HgS on the perfect CeO_2(111) surface is investigated.

HgS is placed on the different adsorption sites on the perfect CeO_2(111) surface with different interaction modes, including Hg up, Hg down, or parallel to the surface. The optimized adsorption structures and the corresponding adsorption energies are shown in Fig. 3 and Table 1. Molecular and dissociated adsorption modes for HgS are obtained. HgS(a) and (b) are two dissociated adsorption configurations with weak interaction with surfaces, in which Hg—S bonds are elongated and cleaved, and the adsorption energies are only −53.6 and −41.1 kJ mol^{-1}. HgS(c), (d) and (e) are three molecular adsorption configurations with medium interaction strength with surfaces. However, S adsorbs on the surface at Ce—O bridge and Ce—Ce bridge sites, while Hg desorbs from the surfaces when HgS is placed with S down or parallel to the O—O bridge site, shown in HgS(f), (g) and (h). They are with higher adsorption energies than that of former five configurations, and bond lengths between S and Hg are elongated from 2.280 Å in gas phase to 3.637, 3.125 and 3.079 Å, respectively. The adsorption mode with Hg desorbing from surface is unfavorable for the removal of Hg.

Mn and Fe modified materials can promote the removal efficiency of Hg [59,60]. Therefore, the adsorption of Hg and the oxidation of Hg by H_2S on the Mn/CeO_2(111) and Fe/CeO_2(111) surfaces will be investigated in the following sections.

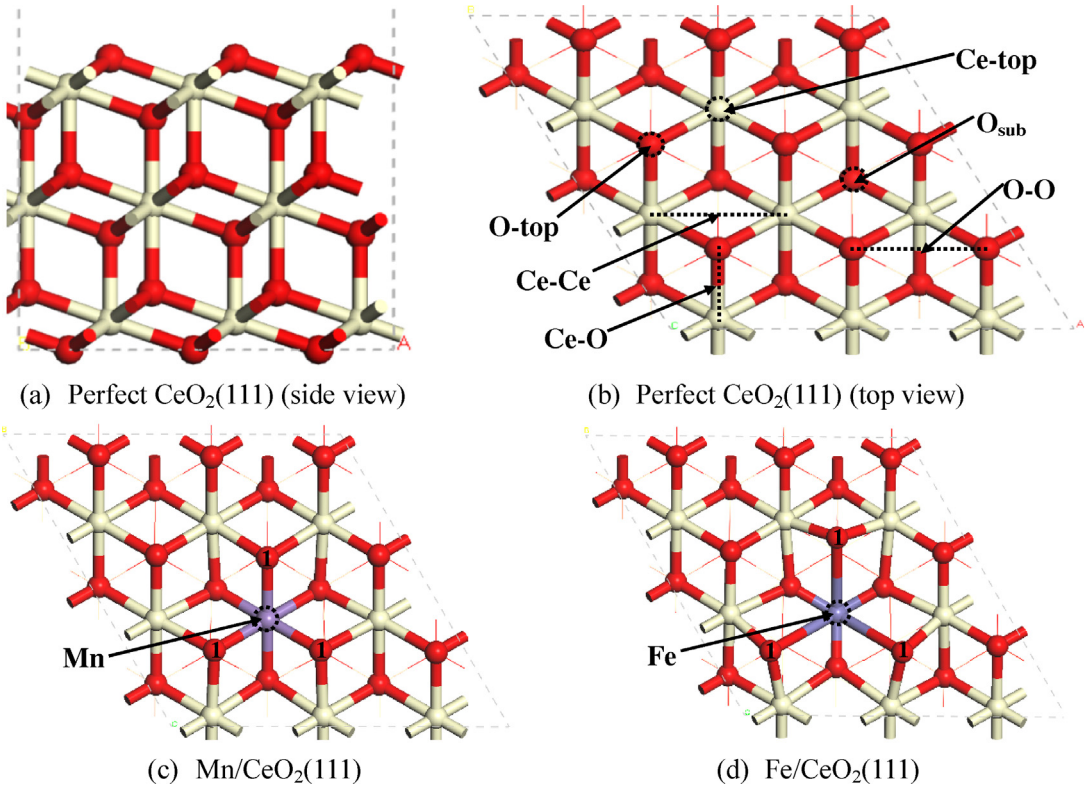

Fig. 1. (a) Side view and (b) top view of the perfect CeO_2(111) surface; (c) Mn-doped CeO_2(111) surface; (d) Fe-doped CeO_2(111) surface. (Red and yellow spheres represent O and Ce atoms, respectively.). (For interpretation of the references to colour in this figure legend, the reader is referred to the web version of this article.)

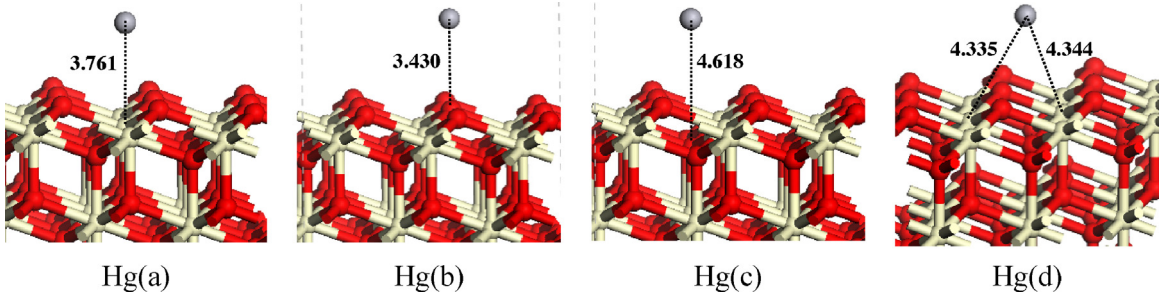

Fig. 2. The adsorption configurations of Hg on the perfect CeO_2(111) surface.

3.2. Adsorption and oxidation of Hg on the Mn/CeO_2 (111) surface

The adsorptions of Hg, HgS and H_2S on the Mn/CeO_2(111) surface will be studied, the adsorption configurations are shown in Fig. 4, and the corresponding adsorption energies are listed in Table 2. In addition, the oxidation of Hg by active S leading to the formation of HgS on the Mn/CeO_2(111) surface will also be studied in this section.

3.2.1. Adsorption of Hg on the Mn/CeO_2(111) surface

Three stable adsorption configurations of Hg on the Mn/CeO_2(111) surface are obtained. In Mn_Hg(a), Hg atom interacts with the doped Mn atom, and the Hg-Mn bond is 3.031 Å, with the adsorption energy −122.7 kJ mol^{-1}. The adsorbed Hg atom bonds with the surface O1 with a bond length of 2.225 Å in Mn_Hg(b), and the adsorption energy is −51.9 kJ mol^{-1}. For the configuration of Mn_Hg(c), the Hg atom adsorbs on the bridge O1—O1 bond, as well as bonds with the doped Mn atom, and the formed Hg—O and Hg—Mn bonds are 2.071, 2.072 and 2.806 Å, respectively. Hg is with the highest adsorption energy of −156.5 kJ mol^{-1}, which is greatly higher than that on the perfect CeO_2(111) surface. It can be concluded that the Mn dopant strengthens the adsorption Hg on the CeO_2(111) surface.

3.2.2. Adsorption of HgS on the Mn/CeO_2 (111) surface

Molecular and dissociative configurations of HgS adsorption on the Mn/CeO_2(111) surface are obtained, as shown in Fig. 4. In Mn_HgS(a) and (b), HgS adsorbs on the O1—O2 bridge site with different interaction modes, and the adsorption energies are −387.1 and −389.6 kJ mol^{-1}, respectively. The Hg—S bonds are 2.402 and 2.399 Å, which shows these are molecular adsorptions. For Mn_HgS(c) and (d), HgS dissociatively adsorb on the surface, with S bonding with the surface O1 and Hg desorbing from the surface. The S—O1 bonds are 1.621 and 1.610 Å, and the broken Hg-S bonds are 2.919 and 3.257 Å, respectively. The adsorption energies are −394.0 and −364.2 kJ mol^{-1}. The most stable adsorption configuration of HgS on the Mn/CeO_2(111) surface is Mn_HgS(e), which is with the adsorption energy of −485.8 kJ mol^{-1}. In this structure, HgS molecularly adsorbs at the O1—O1 site over the doped Mn atom, and formed Hg—O1 and S—O1 bonds are 2.077 and 1.643 Å.

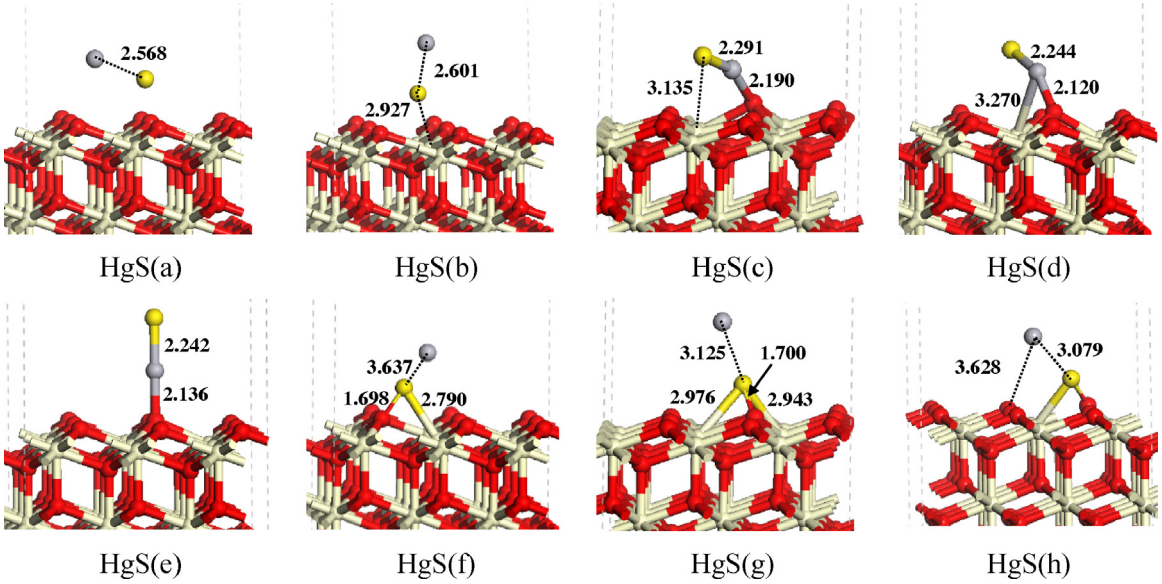

Fig. 3. The adsorption structures of HgS on the perfect $CeO_2(111)$ surface.

Table 2
The adsorption energies of Hg, HgS and H_2S on the $Mn/CeO_2(111)$ surfaces.

Hg	E_{ads}(kJ mol^{-1})	HgS	E_{ads}(kJ mol^{-1})	H_2S	E_{ads}(kJ mol^{-1})
Mn_Hg(a)	−122.7	Mn_HgS(a)	−387.1	Mn_H_2S(a)	−68.1
Mn_Hg(b)	−51.9	Mn_HgS(b)	−389.6	Mn_H_2S(b)	−93.9
Mn_Hg(c)	−156.5	Mn_HgS(c)	−394.0	Mn_H_2S(c)	−42.2
		Mn_HgS(d)	−364.2	Mn_H_2S(d)	−350.3
		Mn_HgS(e)	−485.8	Mn_H_2S(e)	−95.7
		Mn_HgS(f)	−268.1	Mn_H_2S(f)	−174.9
		Mn_HgS(g)	−332.4	Mn_H_2S(g)	−428.6

In Mn_HgS(f) and (g), HgS molecule bonds with its Hg end down to the surface O1 with different angles to the surface. The adsorption energies are −268.1 and −332.4 kJ mol^{-1}.

It can be seen that HgS is mainly molecularly adsorbed on the $Mn/CeO_2(111)$ surface, which is different with that on the perfect $CeO_2(111)$ surface with dissociative mode. We can also see that HgS may be another Hg-containing species on the $Mn/CeO_2(111)$ surface. In the experiment of Hg removal with H_2S in mixture gas, HgS was observed over the iron oxide sorbent [56]. Therefore, the adsorption of H_2S and the formation process of HgS will be studied.

3.2.3. Adsorption of H_2S on the Mn/CeO_2 (111) surface

Three types of adsorption configurations of H_2S on the $Mn/CeO_2(111)$ surface is obtained, including molecular, partial dissociative and complete dissociative modes. Mn_H_2S(a), (b) and (c) are molecular adsorptions of H_2S on the surface, and the adsorption energies are −68.1, −93.9 and −42.2 kJ mol^{-1}. For the partial dissociative adsorption configurations, Mn_H_2S(d) is that dissociated SH and H adsorb on two surface O1 sites with an adsorption energy of −350.3 kJ mol^{-1}. The formed H—O1 and S—O1 bonds are 0.974 and 1.636 Å, and the cleaved S-H bond is 2.832 Å. However, the dissociated SH group desorbs from the surface in Mn_H_2S(e) and (f), and the dissociated H adsorbs on the surface O1 site. The cleaved S-H bonds are 2.263 and 2.339 Å, and the adsorption energies are −95.7 and −174.9 kJ mol^{-1}. When H_2S is placed at the top of the V-shape of O1—Mn—O1, and the V-shape of H—S—H in H_2S overlaps with the O1—Mn—O1 from the top view, H_2S is completely dissociated, as Mn_H_2S(g). The dissociated S bonds with the Mn-O1 bond, and two dissociated H atoms adsorb on the surface O1. The cleaved S-H bonds are 2.360 and 2.460 Å, and the adsorption energy is −428.6 kJ mol^{-1}, which is the most stable structure for the adsorption of H_2S on the $Mn/CeO_2(111)$ surface. It shows that H_2S is easily dissociated and active S can be formed on the surface. However, H_2S adsorbs on the perfect $CeO_2(111)$ surface via molecular mode, and then two little activation energies of 8.0 and 35.2 kJ mol^{-1} are needed for the dissociation of H_2S and SH [13]. On the $ZnO(10\bar{1}0)$ surface, partial dissociated H_2S adsorbs on the surface, and 51.5 kJ mol^{-1} is needed to overcome for the dissociation of SH to S and H [61].

3.2.4. The oxidation of Hg on the $Mn/CeO_2(111)$ surface

Active S can easily be formed and HgS can be existed on the $Mn/CeO_2(111)$ surface. If Hg can be oxidized by active S leading to HgS with low energy barrier, which will promote the removal of mercury. So the oxidation mechanism of Hg is investigated. The co-adsorption structure of S and Hg is as the reactant, which is shown as LM1 in Fig. 5, and the most stable configuration Mn_HgS(e) is as the product. A little energy barrier of 15.4 kJ mol^{-1} is needed to overcome for the formation of HgS, and which is an exothermal process with an energy of −125.8 kJ mol^{-1}. It can be concluded that Hg is easily oxidized by the dissociated active S leading to the formation of HgS on the $Mn/CeO_2(111)$ surface, which is favorable for the simultaneous removal of H_2S and Hg in coal gas. In this process, the adsorbed Hg reacts with the adsorbed S leading to the product HgS, which is followed the Langmuir-Hinshlwood mechanism [62–64]. Therefore, CeO_2 doped with Mn is an effective removal sorbent for H_2S and Hg.

3.3. Adsorption and oxidation of Hg on the Fe/CeO_2 (111) surface

The transition metal Fe is the ideal modified element, which is widely used in the modern catalytic industry to improve the

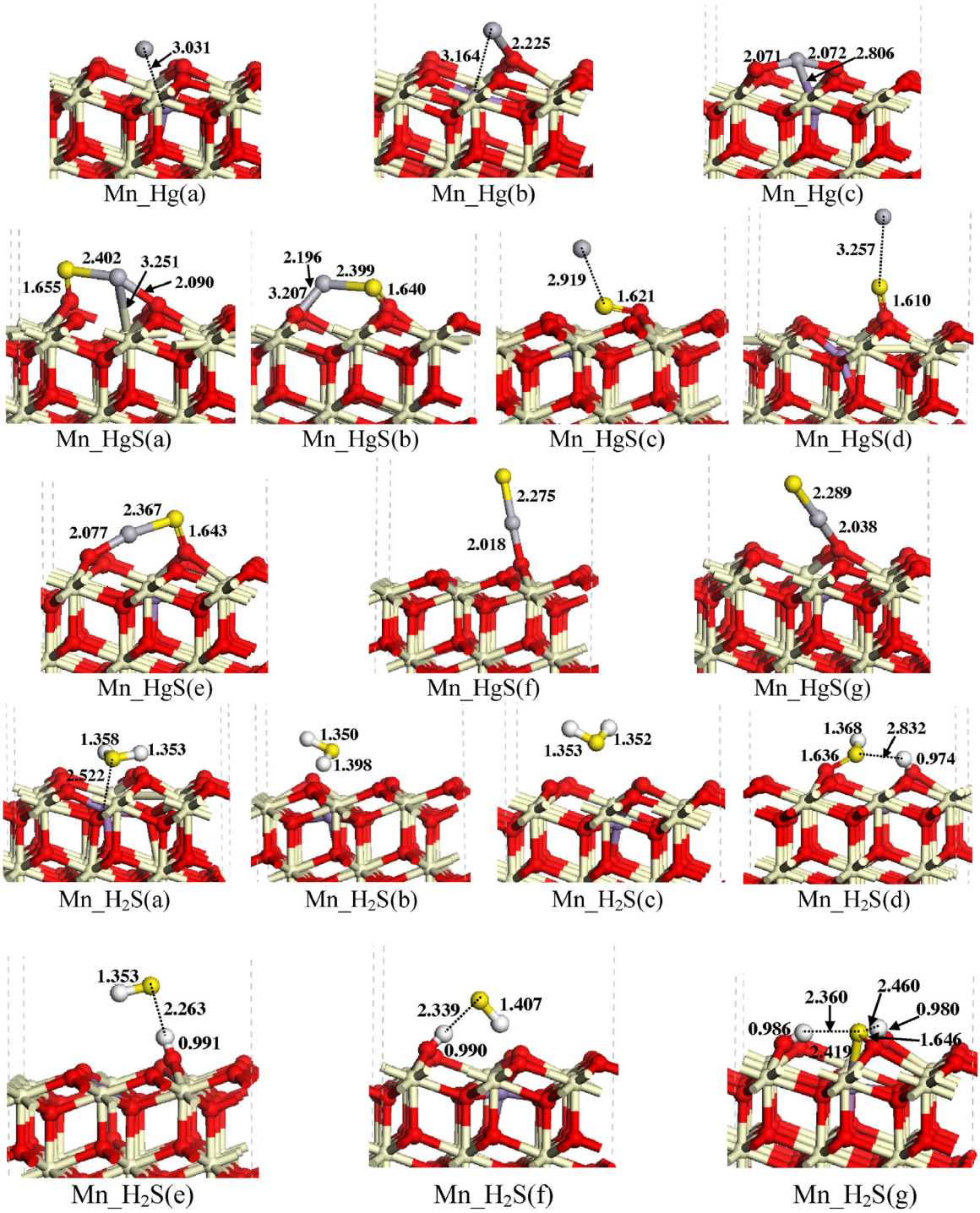

Fig. 4. The adsorption structures of Hg, HgS and H_2S on the Mn/CeO_2(111) surfaces.

Table 3
The adsorption energies of Hg, HgS and H_2S on the Fe/CeO_2(111) surfaces.

Hg	E_{ads}(kJ mol^{-1})	HgS	E_{ads}(kJ mol^{-1})	H_2S	E_{ads}(kJ mol^{-1})
Fe_Hg	−97.2	Fe_HgS(a)	−274.7	Fe_H_2S(a)	−52.2
		Fe_HgS(b)	−318.6	Fe_H_2S(b)	−51.7
		Fe_HgS(c)	−300.2	Fe_H_2S(c)	−205.1
		Fe_HgS(d)	−460.8	Fe_H_2S(d)	−176.4
		Fe_HgS(e)	−357.2	Fe_H_2S(e)	−124.4
		Fe_HgS(f)	−339.4	Fe_H_2S(f)	−413.3
		Fe_HgS(g)	−378.5	Fe_H_2S(g)	−269.3

catalytic properties of CeO_2 [24,25,65], such as promoting the conversion of methane and improving the selectivity of CO and H_2 [23,25]. To investigate the simultaneous removal capacity for Hg and H_2S, the adsorptions of Hg, HgS and H_2S on the Fe/CeO_2(111) surface will be first studied, the adsorption configurations and the corresponding adsorption energies are shown in Fig. 6 and Table 3, respectively. And then, the catalytic oxidation of Hg on the Fe/CeO_2(111) surface will be investigated.

3.3.1. Adsorption of Hg on the Fe/CeO_2 (111) surface

Hg prefers to adsorb on the Fe-top site on the Fe/CeO_2(111) surface, and the formed Fe—Hg bond is 2.847 Å. This adsorption is similar to the case that methane is found to adsorb and activate on the surface iron sites during the oxidation of methane to syngas over Ce-Fe mix oxides [23]. The adsorption energy is −97.2 kJ mol^{-1}, which is lower than that on the Mn/CeO_2(111) surface. However, the adsorptions of Hg are enhanced on the Mn/CeO_2(111) and Fe/CeO_2(111) surfaces comparing with that on the prefect surface. It is similar that the adsorption of CO on the Fe-doped CeO_2(111) surface with higher adsorption energy than that on the perfect CeO_2(111) surface [66]. In addition, NO_2 adsorbs more strongly on the M-doped CeO_2 (M = Mn, Fe) surfaces compared with the undoped surface via the formation of an adsorbed nitrate-like (NO_3^-) species, and the highest adsorption energies for NO_3^- on the CeO_2(111), Mn/CeO_2(111) and Fe/CeO_2(111) surfaces are −105.2, −192.0, and −158.2 kJ mol^{-1} [10]. Additionally, Fe and Mn doped CeO_2(110) are also benefit for the NH_3 adsorption [20].

3.3.2. Adsorption of HgS on the Fe/CeO_2 (111) surface

Similar to the adsorption of HgS on the Mn/CeO_2(111) surface, molecular and dissociative adsorption configurations are obtained. Among all the structures, the most stable one is Fe_HgS(d), in which HgS adsorbs at the O1—O1 bridge site in molecular form, and the formed Hg—O1 and S—O1 bonds are 2.073 and 1.639 Å. The adsorption energy is −460.8 kJ mol^{-1}, which is a strong chemical adsorption, implying that HgS can be captured by the Fe/CeO_2(111) sorbent. HgS was also detected over the iron-based sorbents [56].

In the coal gas, elemental Hg is the main existing form in different Hg-containing species [67]. H_2S is also a main S-containing species [68]. The oxidation of Hg to HgS is one of effective removal mercury methods [52]. The same research method as that on the Mn/CeO_2(111) surface is carried out.

3.3.3. Adsorption of H_2S on the Fe/CeO_2(111) surface

Molecular, partial dissociative and complete dissociative configurations of H_2S on the Fe/CeO_2(111) surface are obtained. Comparing with the adsorption energies of different adsorption structures, we can see that the complete dissociative one is the most stable, as shown in Fe_H_2S(f) and (g), which is similar to that on the Mn/CeO_2(111)surface. Additionally, the doping of Fe was found to promote the decomposition of N_2O [69]. In Fe_H_2S(f) and (g), two dissociated H atoms adsorb on the surface O1, and the dissociated S bonds with the Fe-O1 bond and Fe atom, respectively. The adsorption energies are −413.3 and −269.3 kJ mol^{-1}. It also shows that the active S can be got via the dissociation of H_2S on the Fe/CeO_2(111) surface.

3.3.4. The oxidation of Hg on the Fe/CeO_2 (111) surface

The oxidation process of Hg by the active S via the dissociation of H_2S on the Fe/CeO_2(111) surface is studied. When S is placed at the adjacent Ce-O bridge site to the adsorbed Hg, HgS is formed after optimizing. Therefore, the active S atom is placed at another Ce-O bridge site, which is a little far from the adsorbed Hg. The co-adsorbed structure on the Fe/CeO_2(111) surface is obtained after optimizing, as LM2 in Fig. 7. And then, the adsorbed species react and form HgS with the activation energy of 19.1 kJ mol^{-1} via the Langmuir-Hinshlwood mechanism [62–64]. The low energy barrier makes the HgS formation very easy. It can also be concluded that Fe doped CeO_2 is efficient to remove H_2S and Hg in coal gas simultaneously.

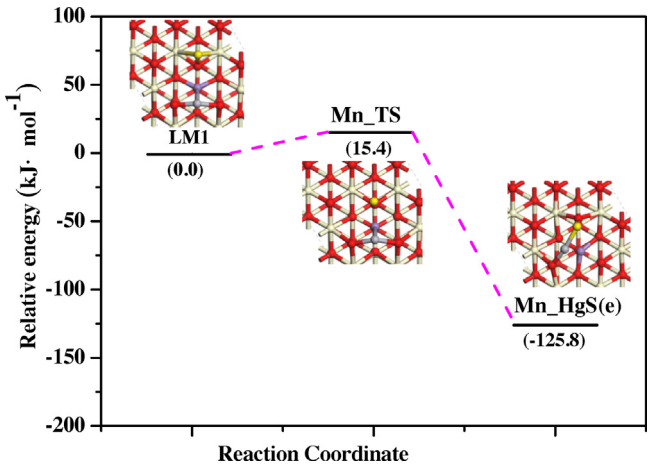

Fig. 5. Schematic potential energy profiles for the oxidation of Hg oxidation by S via the dissociation of H_2S on the Mn/CeO_2(111)surface.

3.4. Effect of metal doping on the removal of mercury

The effect of metal doping on adsorptions of Hg-containing species is first discussed. The doping of Mn and Fe on the CeO_2(111) surface favors the adsorption of Hg. The adsorption of Hg on the perfect CeO_2(111) surface is weak physical interaction with a little energy of −4.6 kJ mol^{-1}, while strong chemical adsorptions are for Hg on Mn/CeO_2(111) and Fe/CeO_2(111) surfaces with adsorption energies of −156.5 and −97.2 kJ mol^{-1}. It indicates the order of interaction strength between Hg and different surfaces is Mn/CeO_2(111)> Fe/CeO_2(111)> CeO_2(111). The Bader charge analysis also show the same order of the interaction strength as shown in Table 4, and 0.013 e, 0.741 e and 0.397 e transfer from Hg atom to the perfect CeO_2(111), Mn/CeO_2(111) and Fe/CeO_2(111) surfaces after interacting, respectively. Besides, the adsorption mode of HgS is changed by doping Mn and Fe on the CeO_2(111) surface. The dissociated adsorption of HgS mainly exists on the perfect CeO_2(111) surface with S binding to the surface and Hg desorbing from surface, which is disadvantage of the removal of Hg. The charge of Hg atom is 0.037 e after HgS adsorbing on the perfect CeO_2(111) surface, which is much close to the charge of Hg in gas phase with 0.000 e, implying that Hg desorbs from the surface. While molecular HgS adsorbs on Mn/CeO_2(111) and Fe/CeO_2(111) surfaces with high adsorption energies when HgS is with the same original structure as that on the perfect surface, which shows that oxidized mercury can be captured by metal doped CeO_2. In addition, much charges transfer from HgS molecule to Mn/CeO_2(111) and Fe/CeO_2(111) surfaces as shown in Table 4. It can be seen that HgS species can be stabilized on Mn/CeO_2(111) and Fe/CeO_2(111) surfaces, which are similar that some intermediate species including C_3 can be stabilized via unpaired electrons delocalizing across the adsorbate and adsorbate-surface bonds, therefore lead to more rapid oxidation during the catalytic propane reforming [29].

In addition, Hg and H_2S can be simultaneously removed by the dissociated S reacting with adsorbed Hg on Mn/CeO_2(111) and Fe/CeO_2(111) surfaces, and two little energy barriers of 15.4 and 19.1 kJ mol^{-1} are needed to overcome. It can be seen that doping Mn and Fe on the CeO_2(111) surface has a positive effect on the simultaneous removal of Hg and H_2S, and HgS is formed via Langmuir-Hinshlwood mechanism. Other metal oxides surfaces

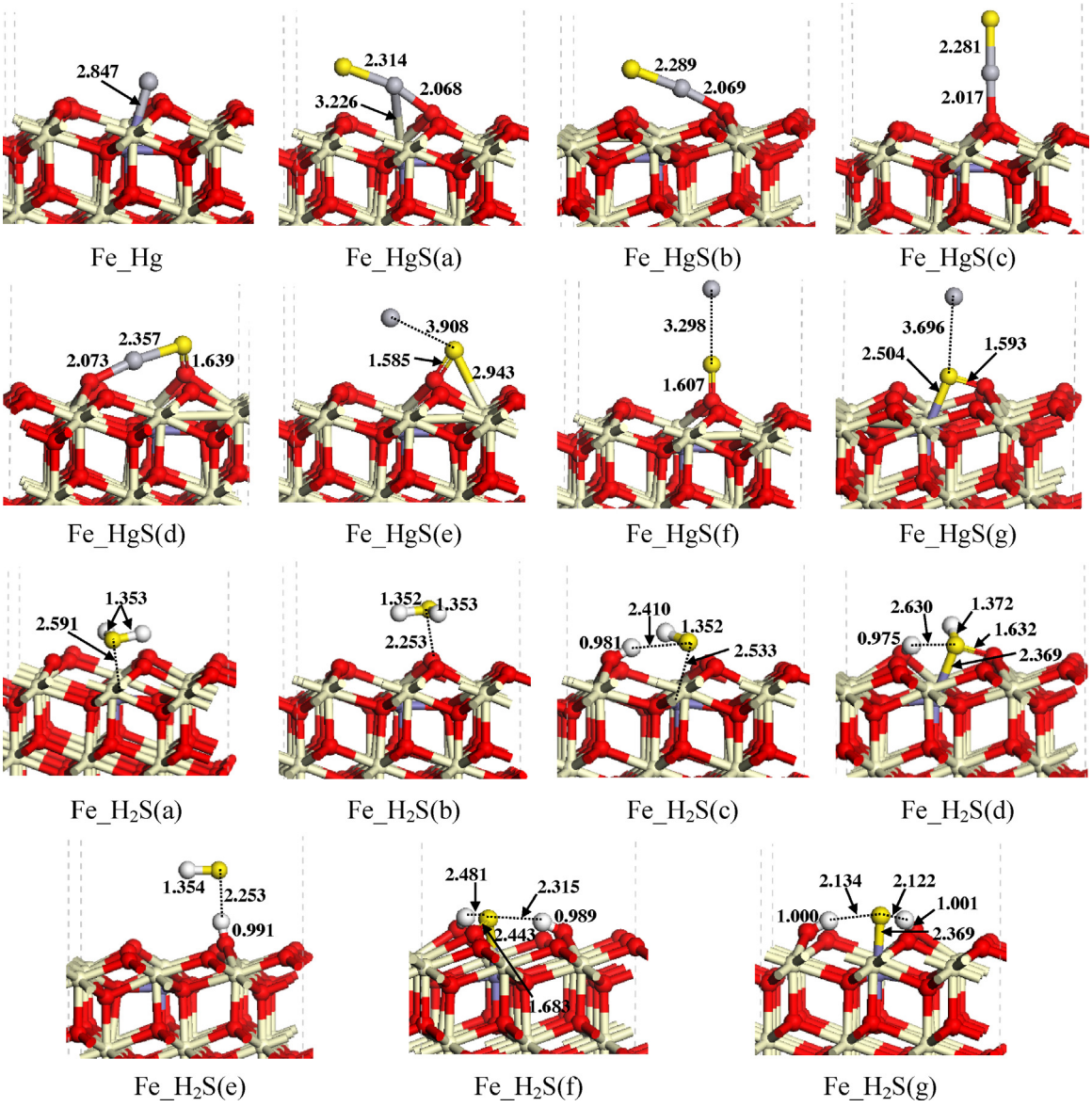

Fig. 6. The adsorption structures of Hg, HgS and H_2S on the Fe/CeO_2(111) surfaces.

have the same function on the simultaneous remove. H_2S can promote the efficiency of Hg adsorption, and Eley-Rideal mechanism was verified as the only possible mechanism for the formation of HgS via Hg adsorption on H_2S/α-Fe_2O_3 surface [70]. Our previous work also showed that the perfect ZnO($10\bar{1}0$) surface is efficient to remove H_2S and Hg simultaneously and H_2S is indispensable to remove Hg [52]. In addition, the temperature-programmed decomposition (TPD) analysis and X-ray photoelectron spectroscopy (XPS) characterization were employed to investigate the Hg removal mechanism in the presence of H_2S over CeO_2 supported on TiO_2 sorbent, and it was found that Hg reacts with active surface sulfur resulting in the formation of HgS [21,71].

4. Conclusion

The simultaneous removal of Hg and H_2S over ceria-based catalysts was studied, and the effects of doped Mn and Fe on adsorptions of Hg-containing species and the reaction of Hg and H_2S was also discussed. Mn and Fe doped CeO_2(111) surfaces were found to be promotional on Hg capture because of stronger interaction between Hg and M/CeO_2(111) (M = Mn, Fe) than that on the perfect surface. HgS molecule can stably exist on Mn and Fe/CeO_2(111) surfaces, while which preferred to exist on the perfect CeO_2(111) surface with dissociated mode.

Table 4
The charge transfer between Hg-containing species and different ceria surfaces.

	Hg on different surfaces		HgS on different surfaces		
	Charge of Hg/e	Charge transfer of Hg/e	Charge of Hg/e	Charge of S/e	Charge transfer of HgS/e
CeO_2(111)	0.013	0.013	0.037	−0.054	−0.017
Mn/CeO_2(111)	0.741	0.741	0.522	0.341	0.863
Fe/CeO_2(111)	0.397	0.397	0.541	0.354	0.895

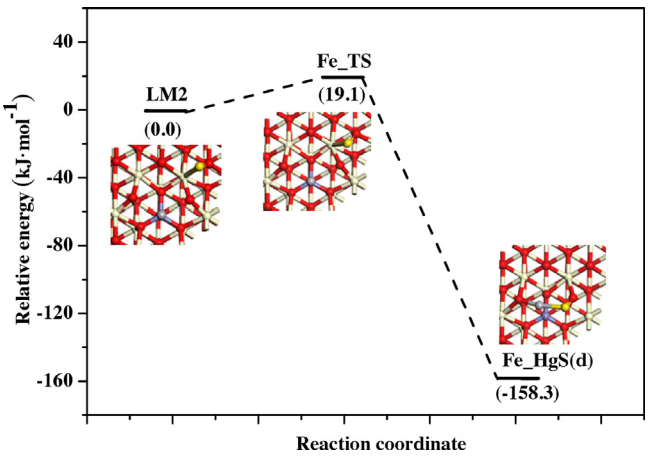

Fig. 7. Schematic potential energy profiles for the oxidation of Hg oxidation by S via the dissociation of H_2S on the Fe/CeO_2(111) surface.

Additionally, the reaction mechanism between Hg and H_2S was investigated to test the simultaneous removal property of Mn and Fe doped CeO_2. The result shows that doping Mn and Fe on the CeO_2(111) surface favors the simultaneous removal of Hg and H_2S. Two little energy barriers of 15.4 and 19.1 kJ mol^{-1} are needed to overcome for the dissociated S reacting with adsorbed Hg on Mn/CeO_2(111) and Fe/CeO_2(111) surfaces.

Acknowledgments

We gratefully acknowledge financial support from the National Natural Science Foundation of China (Grant Nos. 21276171, 21576178 and 21476155), Research Project Supported by Shanxi Scholarship Council of China (No. 2016-030) and the Program for the Innovative Talents of Higher Learning Institutions of Shanxi.

References

[1] Y. Gao, Z. Zhang, J. Wu, L. Duan, A. Umar, L. Sun, Z. Guo, Q. Wang, A critical review on the heterogeneous catalytic oxidation of elemental mercury in flue gases, Environ. Sci. Technol. 47 (2013) 10813–10823.
[2] L. Ling, M. Fan, B. Wang, R. Zhang, Application of computational chemistry in understanding the mechanisms of mercury removal technologies: a review, Energy Environ. Sci. 8 (2015) 3109–3133.
[3] J. Wilcox, E. Rupp, S.C. Ying, D.H. Lim, A.S. Negreira, A. Kirchofer, F. Feng, K. Lee, Mercury adsorption and oxidation in coal combustion and gasification processes, Int. J. Coal Geol. 90–91 (2012) 4–20.
[4] R. Bassilakis, Y. Zhao, P.R. Solomon, M.A. Serio, Sulfur and nitrogen evolution in the argonne coals: experiment and modeling, Energy Fuels 7 (1993) 710–720.
[5] L.X. Han Lv, J. Wang, L. Chang, Palladium–iron bimetal sorbents for simultaneous capture of hydrogen sulfide and mercury from simulated syngas, Energy Fuels 26 (2012) 1638–1644.
[6] Y.H. Li, C.W. Lee, B.K. Gullett, Importance of activated carbon's oxygen surface functional groups on elemental mercury adsorption, Fuel 82 (2003) 451–457.
[7] J.H. Pavlish, M.J. Holmes, S.A. Benson, C.R. Crocker, K.C. Galbreath, Application of sorbents for mercury control for utilities burning lignite coal, Fuel Process. Technol. 85 (2004) 563–576.
[8] S. Cheah, D.L. Carpenter, K.A. Magrini-Bair, Review of mid- to high-temperature sulfur sorbents for desulfurization of biomass- and coal-derived syngas, Energy Fuels 23 (2009) 5291–5307.
[9] H. Wang, Z. Qu, H. Xie, N. Maeda, L. Miao, Z. Wang, Insight into the mesoporous $Fe_xCe_{1-x}O_{2-\delta}$ catalysts for selective catalytic reduction of NO with NH_3: regulable structure and activity, J. Catal. 338 (2016) 56–67.
[10] Y.H. Lu, H.T. Chen, Computational investigation of NO_2 adsorption and reduction on ceria and M-doped CeO_2 (111) (M=Mn, Fe) surfaces, J. Phys. Chem. C 118 (2014) 10043–10052.
[11] M.S. Hegde, P. Bera, Noble metal ion substituted CeO_2 catalysts: electronic interaction between noble metal ions and CeO_2 lattice, Catal. Today 253 (2015) 40–50.
[12] Y. Zeng, S. Kaytakoglu, D. Harrison, Reduced cerium oxide as an efficient and durable high temperature desulfurization sorbent, Chem. Eng. Sci 55 (2000) 4893–4900.
[13] H.T. Chen, Y. Choi, M. Liu, M.C. Lin, A first-principles analysis for sulfur tolerance of CeO_2 in solid oxide fuel cells, J. Phys. Chem. C 111 (2007) 11117–11122.
[14] M. Flytzani-Stephanopoulos, M. Sakbodin, Z. Wang, Regenerative adsorption and removal of H_2S from hot fuel gas streams by rare earth oxides, Science 312 (2006) 1508–1510.
[15] X. Fan, C. Li, G. Zeng, Z. Gao, L. Chen, W. Zhang, H. Gao, Removal of gas-phase element mercury by activated carbon fiber impregnated with CeO_2, Energy Fuels 24 (2010) 4250–4254.
[16] L. Tian, C. Li, Q. Li, G. Zeng, Z. Gao, S. Li, X. Fan, Removal of elemental mercury by activated carbon impregnated with CeO_2, Fuel 88 (2009) 1687–1691.
[17] X. Fan, C. Li, G. Zeng, X. Zhang, S. Tao, P. Lu, Y. Tan, D. Luo, Hg^0 removal from simulated flue gas over CeO_2/HZSM-5, Energy Fuels 26 (2012) 2082–2089.
[18] X. Wen, C. Li, X. Fan, H. Gao, W. Zhang, L. Chen, G. Zeng, Y. Zhao, Experimental study of gaseous elemental mercury removal with $CeO_2/\gamma.Al_2O_3$, Energy Fuels 25 (2011) 2939–2944.
[19] Y. Wang, F. Wang, Y. Chen, D. Zhang, B. Li, S. Kang, X. Li, L. Cui, Enhanced photocatalytic performance of ordered mesoporous Fe-doped CeO_2 catalysts for the reduction of CO_2 with H_2O under simulated solar irradiation, Appl. Catal. B: Environ. 147 (2014) 602–609.
[20] Y. Peng, W. Yu, W. Su, X. Huang, J. Li, An experimental and DFT study of the adsorption and oxidation of NH_3 on a CeO_2 catalyst modified by Fe, Mn, La and Y, Catal. Today 242 (Part B) (2015) 300–307.
[21] J. Zhou, W. Hou, P. Qi, X. Gao, Z. Luo, K. Cen, CeO_2-TiO_2 sorbents for the removal of elemental mercury from syngas, Environ. Sci. Technol. 47 (2013) 10056–10062.
[22] L. Bi, H. Kim, G.F. Dionne, S.A. Speakman, D. Bono, C.A. Ross, Structural, magnetic, and magneto-optical properties of Co-doped $CeO_{2-\delta}$ films, J. Appl. Phys. 103 (2008) 07D138.
[23] K. Li, H. Wang, Y. Wei, D. Yan, Syngas production from methane and air via a redox process using Ce?Fe mixed oxides as oxygen carriers, Appl. Catal. B: Environ. 97 (2010) 361–372.
[24] Q.Y. Wen, H.W. Zhang, Q.H. Yang, Y.Q. Song, J.Q. Xiao, Effects of Fe doping and the dielectric constant on the room temperature ferromagnetism of polycrystalline CeO_2 oxides, J. Appl. Phys. 107 (2010) 09C307.
[25] K. Li, H. Wang, Y. Wei, D. Yan, Transformation of methane into synthesis gas using the redox property of Ce?Fe mixed oxides: effect of calcination temperature, Int. J. Hydrogen Energy 36 (2011) 3471–3482.
[26] X.S. Liu, X.D. Wang, M. Yao, W. Cui, H. Yan, Effects of Fe doping on oxygen vacancy formation and CO adsorption and oxidation at the ceria(111) surface, Catal. Commun. 63 (2015) 35–40.
[27] D. García Pintos, A. Juan, B. Irigoyen, Mn-doped CeO_2: DFT + U study of a catalyst for oxidation reactions, J. Phys. Chem. C 117 (2013) 18063–18073.
[28] L. Hsu, M. Tsai, Y. Lu, H. Chen, Computational investigation of CO adsorption and oxidation on Mn/CeO_2(111) surface, J. Phys. Chem. C 117 (2013) 433–441.
[29] M.D. Krcha, M.J. Janik, Catalytic propane reforming mechanism over Mn-Doped CeO_2 (111), Surf. Sci. 640 (2015) 119–126.
[30] D. Qiao, G. Lu, X. Liu, Y. Guo, Y. Wang, Y. Guo, Preparation of Ce_{1-x} Fe $_x$ O_2 solid solution and its catalytic performance for oxidation of CH_4 and CO, J. Mater. Sci. 46 (2011) 3500–3506.
[31] G. Kresse, J. Furthmüller, Efficient iterative schemes for ab initio total-energy calculations using a plane-wave basis set, Phys. Rev. B 54 (1996) 11169.
[32] G. Sun, J. Kürti, P. Rajczy, M. Kertesz, J. Hafner, G. Kresse, Performance of the Vienna ab initio simulation package (VASP) in chemical applications, J. Mol. Struct.: Theochem. 624 (2003) 37–45.
[33] J.P. Perdew, K. Burke, M. Ernzerhof, Generalized gradient approximation made simple, Phys. Rev. Lett. 77 (1996) 3865.
[34] P.E. Blöchl, Projector augmented-wave method, Phys. Rev. B 50 (1994) 17953.
[35] G. Kresse, D. Joubert, From ultrasoft pseudopotentials to the projector augmented-wave method, Phys. Rev. B 59 (1999) 1758.
[36] J. Zhang, X.Q. Gong, G. Lu, Catalytic activities of $CeO_2(110)-2\times1$ reconstructed surface, Surf. Sci. 632 (2015) 164–173.
[37] F. Chen, D. Liu, J. Zhang, P. Hu, X.Q. Gong, G. Lu, A DFT + U study of the lattice oxygen reactivity toward direct CO oxidation on the CeO_2(111) and (110) surfaces, Phys. Chem. Chem. Phys. 14 (2012) 16573–16580.
[38] O. DíAlessandro, D.G. Pintos, A. Juan, B. Irigoyen, J. Sambeth, A DFT study of phenol adsorption on a low doping Mn–Ce composite oxide model, Appl. Surf. Sci. 359 (2015) 14–20.
[39] W. Cen, Y. Liu, Z. Wu, H. Wang, X. Weng, A theoretic insight into the catalytic activity promotion of CeO_2 surfaces by Mn doping, Phys. Chem. Chem. Phys. 14 (2012) 5769–5777.
[40] S. Huang, B.E. Wilson, W.H. Smyrl, D.G. Truhlar, A. Stein, Transition-metal-doped M-Li_8ZrO_6 (M = Mn, Fe, Co, Ni, Cu, Ce) as high-specific-capacity li-ion battery cathode materials: synthesis, electrochemistry, and quantum mechanical characterization, Chem. Mater. 28 (2016) 746–755.
[41] P. Liao, J.A. Keith, E.A. Carter, Water oxidation on pure and doped hematite (0001) surfaces: prediction of Co and Ni as effective dopants for electrocatalysis, J. Am. Chem. Soc. 134 (2012) 13296–13309.
[42] L. Gerward, J.S. Olsen, Powder diffraction analysis of cerium dioxide at high pressure, Powder Diffr. 8 (1993) 127–129.
[43] H.T. Chen, Y.M. Choi, M. Liu, M. Lin, A theoretical study of surface reduction mechanisms of CeO_2(111) and (110) by H_2, Chemphyschem.: Eur. J. Chem. Phys. Phys. Chem. 8 (2007) 849–855.

[44] W. Wang, S. Thevuthasan, W. Wang, P. Yang, Theoretical study of trimethylacetic acid adsorption on CeO_2(111) surface, J. Phys. Chem. C 120 (2016) 2655–2666.
[45] D.R. Lide, CRC Handbook of Chemistry and Physics, 82nd edition, CRC Press, 2001.
[46] G. Henkelman, B.P. Uberuaga, H. Jónsson, A climbing image nudged elastic band method for finding saddle points and minimum energy paths, J. Chem. Phys. 113 (2000) 9901–9904.
[47] G. Henkelman, H. Jónsson, Improved tangent estimate in the nudged elastic band method for finding minimum energy paths and saddle points, J. Chem. Phys. 113 (2000) 9978–9985.
[48] G. Henkelman, H. Joínsson, A dimer method for finding saddle points on high dimensional potential surfaces using only first derivatives, J. Chem. Phys. 111 (1999) 7010.
[49] R.A. Olsen, G.J. Kroes, G. Henkelman, A. Arnaldsson, H. Jonsson, Comparison of methods for finding saddle points without knowledge of the final states, J. Chem. Phys. 121 (2004) 9776–9792.
[50] X. Hua, J. Zhou, Q. Li, Z. Luo, K. Cen, Gas-phase elemental mercury removal by CeO_2 impregnated activated coke, Energy Fuels 24 (2010) 5426–5431.
[51] B. Zhang, J. Liu, F. Shen, Heterogeneous mercury oxidation by HCl over CeO_2 catalyst: density functional theory study, J. Phys. Chem. C 119 (2015) 15047–15055.
[52] L. Ling, P. Han, B. Wang, R. Zhang, Theoretical prediction of simultaneous removal efficiency of ZnO for H_2S and Hg^0 in coal gas, Chem. Eng. J. 231 (2013) 388–396.
[53] P. Guo, X. Guo, C. Zheng, Computational insights into interactions between Hg species and α-Fe_2O_3(0 0 1), Fuel 90 (2011) 1840–1846.
[54] W. Xiang, J. Liu, M. Chang, C. Zheng, The adsorption mechanism of elemental mercury on CuO (110) surface, Chem. Eng. J. 200 (2012) 91–96.
[55] S. Sun, D. Zhang, C. Li, Y. Wang, Q. Yang, Density functional theory study of mercury adsorption and oxidation on CuO (111) surface, Chem. Eng. J. 258 (2014) 128–135.
[56] S. Wu, M. Azhar Uddin, E. Sasaoka, Characteristics of the removal of mercury vapor in coal derived fuel gas over iron oxide sorbents, Fuel 85 (2006) 213–218.
[57] M. Ozaki, M.A. Uddin, E. Sasaoka, S. Wu, Temperature programmed decomposition desorption of the mercury species over spent iron-based sorbents for mercury removal from coal derived fuel gas, Fuel 87 (2008) 3610–3615.
[58] J. Wang, Y. Zhang, L. Han, L. Chang, W. Bao, Simultaneous removal of hydrogen sulfide and mercury from simulated syngas by iron-based sorbents, Fuel 103 (2013) 73–79.
[59] L. Xing, Y. Xu, Q. Zhong, Mn and Fe modified fly ash as a superior catalyst for elemental mercury capture under air conditions, Energy Fuels 26 (2012) 4903–4909.
[60] H. Li, C.Y. Wu, Y. Li, J. Zhang, Superior activity of MnO_x-CeO_2/TiO_2 catalyst for catalytic oxidation of elemental mercury at low flue gas temperatures, Appl. Catal. B: Environ. 111–112 (2012) 381–388.
[61] L. Ling, R. Zhang, P. Han, B. Wang, DFT study on the sulfurization mechanism during the desulfurization of H_2S on the ZnO desulfurizer, Fuel Process. Technol. 106 (2013) 222–230.
[62] A.A. Presto, E.J. Granite, Noble metal catalysts for mercury oxidation in utility flue gas, Platinum Met. Revev 52 (2008) 144–154.
[63] Y. Eom, S.H. Jeon, T.A. Ngo, J. Kim, T.G. Lee, Heterogeneous mercury reaction on a selective catalytic reduction (SCR) catalyst, Catal. Lett. 121 (2008) 219–225.
[64] R.J. Baxter, P. Hu, Insight into why the Langmuir–Hinshelwood mechanism is generally preferred, J. Chem. Phys. 116 (2002) 4379.
[65] K. Li, M. Haneda, M. Ozawa, Oxygen release–absorption properties and structural stability of $Ce_{0.8}Fe_{0.2}O_{2-x}$, J. Mater. Sci. 48 (2013) 5733–5743.
[66] H. Chen, J. Chang, Computational investigation of CO adsorption and oxidation on iron-modified cerium oxide, J. Phys. Chem. C 115 (2011) 14745–14753.
[67] Y. Wang, B. Shen, C. He, S. Yue, F. Wang, Simultaneous removal of NO and Hg^0 from flue gas over Mn–Ce/Ti-PILCs, Environ. Sci. Technol. 49 (2015) 9355–9363.
[68] S. Zhao, L. Ling, B. Wang, R. Zhang, D. Li, Q. Wang, J. Wang, Theoretic insight into the desulfurization mechanism: removal of H_2S by ceria (110), J. Phys. Chem. C 119 (2015) 7678–7688.
[69] F.J. Perez-Alonso, I. Melián-Cabrera, M. López Granados, F. Kapteijn, J.L.G. Fierro, Synergy of $Fe_xCe_{1-x}O_2$ mixed oxides for N_2O decomposition, J. Catal. 239 (2006) 340–346.
[70] L. Tao, X. Guo, C. Zheng, Density functional study of Hg adsorption mechanisms on α-Fe_2O_3 with H_2S, Proc. Combust. Inst. 34 (2013) 2803–2810.
[71] W. Hou, J. Zhou, P. Qi, X. Gao, Z. Luo, Effect of H_2S/HCl on the removal of elemental mercury in syngas over CeO_2–TiO_2, Chem. Eng. J. 241 (2014) 131–137.